Quantum spin ladders of non-Abelian anyons

Didier Poilblanc,[1] Andreas W. W. Ludwig,[2] Simon Trebst,[3] and Matthias Troyer[4]
[1]*Laboratoire de Physique Théorique, CNRS, and Université de Toulouse, F-31062 Toulouse, France*
[2]*Physics Department, University of California, Santa Barbara, California 93106, USA*
[3]*Microsoft Research, Station Q, University of California, Santa Barbara, California 93106, USA*
[4]*Theoretische Physik, ETH Zurich, CH-8093 Zurich, Switzerland*
(Received 15 January 2011; revised manuscript received 13 March 2011; published 29 April 2011)

Quantum ladder models, consisting of coupled chains, form intriguing systems bridging one and two dimensions and have been well studied in the context of quantum magnets and fermionic systems. Here we consider ladder systems made of more exotic quantum mechanical degrees of freedom, so-called non-Abelian anyons, which can be thought of as certain quantum deformations of ordinary SU(2) spins. Such non-Abelian anyons occur as quasiparticle excitations in topological quantum fluids, including $p_x + ip_y$ superconductors, certain fractional quantum Hall states, and rotating Bose-Einstein condensates. Here we use a combination of exact diagonalization and conformal field theory to determine the phase diagrams of ladders with up to four chains. We discuss how phenomena familiar from ordinary SU(2) spin ladders are generalized in their anyonic counterparts, such as gapless and gapped phases, odd and even effects with the ladder width, and elementary "magnon" excitations. Other features are entirely due to the topological nature of the anyonic degrees of freedom. In general, two-dimensional systems of interacting localized non-Abelian anyons are anyonic generalizations of two-dimensional quantum magnets.

DOI: 10.1103/PhysRevB.83.134439 PACS number(s): 74.20.Mn, 67.80.kb, 75.10.Jm

I. INTRODUCTION

Quantum antiferromagnets and, more generally, electronic systems are notoriously known to behave fundamentally differently in one and two spatial dimensions. In one spatial dimension quantum fluctuations are enhanced and often give rise to critical properties such as algebraic spin (or charge) correlations.[1] In contrast, in two spatial dimensions one frequently finds quantum ground states (GSs) with long-range order, which often originate from the spontaneous breaking of a continuous symmetry. The archetypal example of the latter are Heisenberg antiferromagnets on bipartite lattices,[2] where the Néel GS arises from the spontaneous breaking of the SU(2) spin symmetry and the resulting zero-energy Goldstrone modes are spin-wave excitations, also called magnons. Quantum ladder systems, consisting of a finite number W of coupled one-dimensional (1D) systems, form a bridge between between these two limits, and the evolution of quantum GSs in the dimensional crossover of increasing ladder width has been well studied in the context of itinerant bosonic and fermionic systems[3] as well as quantum spin ladders.[4] A variety of remarkable crossover effects have been observed, such as the celebrated even/odd effect in quantum spin-1/2 Heisenberg ladders, where gapless GSs are found for all odd width W, while ladder systems with an even number of legs exhibit a spin gap.[4] Surely, this effect has also been experimentally observed for actual materials realizing almost perfect two- and three-leg $S = 1/2$ antiferromagnetic (AFM) ladders when performing careful magnetic susceptibility measurements.[5]

In this paper, we consider systems of more exotic quantum mechanical degrees of freedom, so-called non-Abelian anyons, which have attracted considerable interest in the description of non-Abelian vortices in unconventional $p_x + ip_y$ superconductors,[6] quasiholes in certain fractional quantum Hall states,[7–9] excitations in certain heterostructures involving a unique class of materials, so-called topological insulators,[10] or vortices in rotating Bose-Einstein condensates,[11] and in theoretical proposals for inherently fault tolerant quantum computing schemes.[12] Since we are interested in their collective quantum GSs in two spatial dimensions, we follow a route similar to the above-mentioned studies of SU(2) quantum antiferromagnets and study ladder systems of interacting anyonic degrees of freedom.

Formally, non-Abelian anyons can be described by so-called $\mathrm{su}(2)_k$ Chern-Simons theories, which correspond to certain quantum deformations[13] of SU(2). In these theories, the non-Abelian degrees of freedoms are captured by "generalized angular momenta" j, which for a given $\mathrm{su}(2)_k$ theory, are constrained to the first $k+1$ representations of SU(2),

$$j = 0, \frac{1}{2}, 1, \frac{3}{2}, \ldots, \frac{k}{2}.$$

Similar to the coupling of ordinary angular momenta, two non-Abelian degrees of freedom can be "fused" into multiple states with total angular momenta (or spin),

$$j_1 \otimes j_2 = |j_1 - j_2| \oplus |j_1 - j_2| + 1 \oplus \cdots \oplus \min(j_1 + j_2, k - j_1 - j_2),$$

where again the "cutoff" k of the deformation enters. The occurrence of *multiple* fusion channels on the right-hand side of the above equation is what intrinsically gives rise to a *macroscopic* degeneracy of states for a set of multiple non-Abelian anyons, i.e., the degeneracy grows exponentially with the number of anyons. This macroscopic degeneracy is the hallmark of non-Abelian statistics.

In this paper we consider the fundamental case of non-Abelian anyons with generalized angular momentum $j = 1/2$, which obey the fusion rule $1/2 \otimes 1/2 = 0 \oplus 1$ reminiscent of two ordinary spin-1/2's coupling into a singlet or triplet. As the Heisenberg Hamiltonian for ordinary spins, interactions

 ©2011 American Physical Society

between the anyons energetically split the two fusion outcomes, which in the case of ordinary SU(2) spins is captured by the familiar Heisenberg Hamiltonian,

$$H = \sum_{i,j} J_{ij} \vec{S}_i \cdot \vec{S}_j \tag{1}$$

$$= \frac{1}{2} \sum_{i,j} J_{ij} [(\vec{S}_i + \vec{S}_j)^2 - \vec{S}_i^2 - \vec{S}_j^2] \tag{2}$$

$$= - \sum_{i,j} J_{ij} \Pi^0_{i,j} + \text{const}, \tag{3}$$

which can be viewed as a sum of pairwise projectors $\Pi^0_{i,j}$ onto the singlet state. Similarly, we can define an "anyonic Heisenberg Hamiltonian" that for a pair of non-Abelian anyons with generalized angular momentum $j = 1/2$ projects onto the $j = 0$ (singlet) fusion channel, thus taking the same form as Eq. (3) of the Hamiltonian above. In analogy to ordinary SU(2) spins we refer to positive couplings (projecting onto the generalized $j = 0$ state) as antiferromagnetic (AFM), while negative couplings (projecting onto the generalized $j = 1$ state) are ferromagnetic (FM).

It has recently been shown that similar to their SU(2) counterparts chains of interacting non-Abelian anyons can exhibit a variety of collective GSs, including stable gapless phases[14–17] and exotic infinite-randomness fixed points.[18–20] In this paper, we aim at understanding *two-dimensional* GSs of interacting non-Abelian anyons and—following a similar route as in the case of the above-mentioned studies of SU(2) quantum antiferromagnets—we consider systems of coupled chains forming W-leg ladders. Employing extensive numerical simulations combined with a conformal field theory analysis, we investigate phase diagrams of W-leg ladder with up to $W = 4$ legs, which allows us to infer some conclusions also for the two-dimensional (2D) limit of $W \to \infty$. We mostly focus on the case of su(2)$_k$ with $k = 3$ as a representative example and in particular all numerical simulations are performed for this case. We will return to the more general case of arbitrary level $k > 3$ in Sec. VI.

While in this paper we detail the physics of interacting non-Abelian anyons mostly in terms of (deformed) quantum spins—a notion more familiar to the field of low-dimensional quantum magnetism—we have put forward another perspective on the physics of interacting anyons in the context of certain fractional quantum Hall states in a recent article.[21] There we have made a connection between the collective states of (anyonic) excitations in non-Abelian quantum Hall liquids and the physics of moving on a non-Abelian quantum Hall plateau.

The remainder of this paper is structured as follows: We will start with a detailed derivation of the microscopic models analyzed in this paper in Sec. II. This is followed by a discussion of the phase diagrams of the various ladder models starting from the strong rung-coupling limit in Sec. III and continuing with the weak rung-coupling limit in Sec. IV. We will then turn to the peculiar role of boundary conditions and the occurrence of gapless modes at open boundaries for these anyonic ladder models in Sec. V. We round off the paper by a discussion of the two-dimensional limit of these ladder models in Sec. VII and generalization to su(2)$_k$ theories with $k > 3$ in Sec. VI.

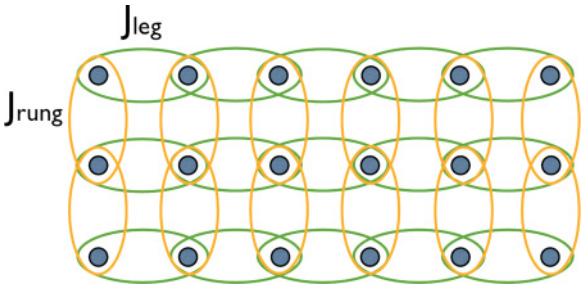

FIG. 1. (Color online) Three coupled chains of interacting anyons (indicated by the filled circles). The interaction along (J_{leg}) and perpendicular (J_{rung}) to the chains are indicated by the ellipses.

II. THE MICROSCOPIC LADDER MODEL

In this section we will give a definition of the microscopic W-leg ladder models for so-called su(2)$_3$ Fibonacci anyons. We will keep our discussion short but self-contained, as an extended derivation of general microscopic Hamiltonians has been given in Ref. 22. We will emphasize in the following those aspects that are not covered in Ref. 22. For a given W-leg ladder we denote the strength of the interactions as J_{leg} and J_{rung} for the coupling along and perpendicular to the chains, respectively, as illustrated in Fig. 1. Parametrizing these couplings as $J_{\text{leg}} = \cos\theta$ and $J_{\text{rung}} = \sin\theta$ we will map out the parameter space on a unit circle as shown in Fig. 2.

Our numerical analysis of these ladder systems is based on exact diagonalization using the Lanczos algorithm, which provides us with the low-energy spectra of finite systems with extent $W \times L$, where L is the length of the ladder in the chain direction and W is the width of the ladder in the rung direction.

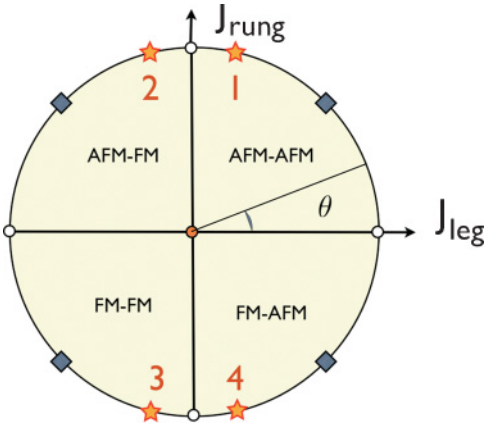

FIG. 2. (Color online) Representation of the parameter space of the model on a circle. The couplings J_{rung} and J_{leg} can be either positive (AFM) or negative (FM). The different phases in each of the quadrants labeled by J_{rung}–J_{leg} are given in Table I. The (gray) squares at $\pi/4$ correspond to isotropic couplings $|J_{\text{rung}}/J_{\text{leg}}| = 1$. The (orange) stars mark the parameters in the vicinity of the strong-coupling limit $|J_{\text{rung}}| \gg |J_{\text{leg}}|$ used in this work, namely, $\theta = \{3\pi/7, 4\pi/7, 10\pi/7, 11\pi/7\}$ labeled from 1 to 4, respectively.

In our exact diagonaliztion studies, we have been able to analyze systems of size $2 \times L$ ($L = 8,12,15,16,18,20,21$), $3 \times L$ ($L = 6,8,9,10,12$) and $4 \times L$ ($L = 4,6,8$).

A. The basis states

To describe the basis states of a set of N localized (interacting) su(2)$_3$ anyons we consider a fusion path, as shown in Fig. 3(a). The basis of the many-anyon Hilbert space corresponds to all admissible labelings $|x_1,x_2,\ldots\rangle$ of the links in this fusion path with labels x_i corresponding to generalized angular momenta of su(2)$_3$. These labelings must satisfy the constraints of the fusion rules at each vertex of this fusion path. For su(2)$_3$ these fusion rules are

$$0 \otimes \alpha = \alpha, \quad 1/2 \otimes 1/2 = 0 \oplus 1, \quad 1/2 \otimes 1 = 1/2 \oplus 3/2,$$
$$1/2 \otimes 3/2 = 1, \quad 1 \otimes 1 = 0 \oplus 1, \quad 1 \otimes 3/2 = 1/2, \qquad (4)$$
$$3/2 \otimes 3/2 = 0,$$

where $\alpha \otimes \beta = \beta \otimes \alpha$. These fusion rules (4) reveal an automorphism $\alpha \to \hat{\alpha} = 3/2 - \alpha$, allowing an identification of $0 \leftrightarrow 3/2$ and $1/2 \leftrightarrow 1$ for su(2)$_3$. Using the notation for the Fibonacci theory, we write the identity $\mathbf{1}$ for the former and the label τ for the latter, thus leading to the fusion rules

$$\mathbf{1} \otimes \mathbf{1} = \mathbf{1}, \quad \mathbf{1} \otimes \tau = \tau, \quad \tau \otimes \tau = \mathbf{1} \oplus \tau. \qquad (5)$$

For the labelings of the fusion path these rules then imply that $x_i = \mathbf{1}$ has to be followed by $x_{i+1} = \tau$ but $x_i = \tau$ can be followed by either $x_{i+1} = \mathbf{1}$ or $x_{i+1} = \tau$. This constraint gives an overall Hilbert space size to $F_{N+1} + F_{N-1} \sim \phi^N$ (for large N) where F is the Fibonacci sequence and $\phi = (1+\sqrt{5})/2$, the golden mean. Note that in comparison to ordinary SU(2) spin-1/2 systems this Hilbert space has a reduced size.

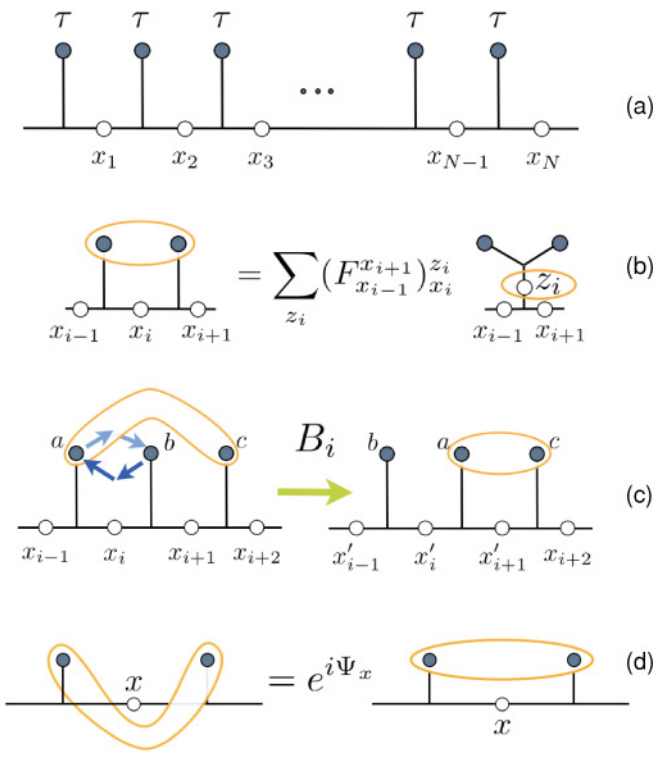

FIG. 3. (Color online) (a) The fusion path connecting N Fibonacci [su(2)$_3$] anyons. Basis states correspond to all admissible labelings of the edges x_i with anyon charges 0 and 1/2 that satisfy the fusion rules. (b) A nearest-neighbor coupling in a chain of anyons can be calculated by using the F matrix to transform to a unique basis in which the fusion product of the two anyons is one of the variables. (c) Longer-range interactions first need to be mapped to nearest-neighbor interaction by braiding anyons. (d) A Dehn twist, giving an additional phase factor is needed if the interaction winds around the torus. For su(2)$_3$ the phase is $\psi_x = 0$ for $x = 0$ and $\psi_x = -4\pi/5$ for $x = 1/2$.

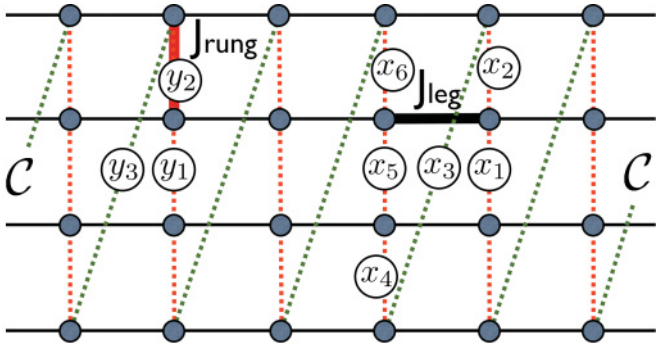

FIG. 4. (Color online) Sketch of a typical ladder system of extent $4 \times L$ ($L = 6$), where the dots indicate the location of τ anyons. The fusion path $\mathcal{C}$ (dotted line) with labelings x_i (or y_i) is used define an (arbitrary) ordering of the sites, which is used in the definition of the basis states. The exchange couplings J_{leg} and J_{rung} are indicated.

B. The rung interactions

With our choice of fusion path the rung coupling J_{rung} on ladders with open boundary conditions on the rungs always connects neighboring anyons along the fusion path. To calculate the interaction between two neighboring anyons as in Fig. 3(b) we need to calculate their total spin by performing a basis transformation using the F matrix, and then assign energy $-J_{\text{rung}}$ to the identity fusion channel and energy 0 to the τ fusion channel. This basis transformation is illustrated in Fig. 3.

Denoting the local basis states on the three edges around the interaction as $|x_{i-1},x_i,x_{i+1}\rangle \in \{|\mathbf{1},\tau,\mathbf{1}\rangle,|\mathbf{1},\tau,\tau\rangle,|\tau,\tau,\mathbf{1}\rangle,|\tau,\mathbf{1},\tau\rangle,|\tau,\tau,\tau\rangle\}$ and the states after the F transformation as $|x_{i-1},z_i,x_{i+1}\rangle \in$

$\{|\mathbf{1},\mathbf{1},\mathbf{1}\rangle,|\mathbf{1},\tau,\tau\rangle,|\tau,\tau,\mathbf{1}\rangle,|\tau,\mathbf{1},\tau\rangle,|\tau,\tau,\tau\rangle\}$, we can write the F matrix as

$$F_i = \begin{bmatrix} 1 & 0 & 0 & 0 & 0 \\ 0 & 1 & 0 & 0 & 0 \\ 0 & 0 & 1 & 0 & 0 \\ 0 & 0 & 0 & 1/\phi & 1/\sqrt{\phi} \\ 0 & 0 & 0 & 1/\sqrt{\phi} & -1/\phi \end{bmatrix}. \quad (6)$$

Assigning an energy -1 to the identity $z_i = \mathbf{1}$ and 0 to $z_i = \tau$ the local Hamiltonian is $\mathcal{H}_i = -F_i P_i F_i$, where P_i is the projector onto the state with $z_i = \mathbf{1}$. In the basis defined above we get

$$\mathcal{H}_i = \begin{bmatrix} -1 & 0 & 0 & 0 & 0 \\ 0 & 0 & 0 & 0 & 0 \\ 0 & 0 & 0 & 0 & 0 \\ 0 & 0 & 0 & -1/\phi^2 & -1/\phi^{3/2} \\ 0 & 0 & 0 & -1/\phi^{3/2} & -1/\phi \end{bmatrix}. \quad (7)$$

The rung Hamiltonian is obtained by multiplying this matrix by J_{rung} and, for the term shown in Fig. 4 acts on the local states $|y_1,y_2,y_3\rangle$.

C. The leg interactions

Te leg couplings shown on Fig. 4, on the other hand, are longer-range interactions and requires "braiding" of anyons as illustrated in Fig. 3(c). Let us first consider a next-nearest-neighbor interaction along a chain. To transform this into a nearest-neighbor interaction we need to change the basis again, this time by braiding the two left anyons in a clockwise manner with a so-called braid matrix B_i acting on the states $|x_{i-1},x_i,x_{i+1}\rangle$. Using the same basis as before this braid matrix can be written as

$$B_i = \begin{bmatrix} e^{4i\pi/5} & 0 & 0 & 0 & 0 \\ 0 & e^{-3i\pi/5} & 0 & 0 & 0 \\ 0 & 0 & e^{-3i\pi/5} & 0 & 0 \\ 0 & 0 & 0 & \frac{1}{\phi^2}e^{4i\pi/5} + \frac{1}{\phi}e^{-3i\pi/5} & \frac{1}{\phi^{3/2}}(e^{4i\pi/5} - e^{-3i\pi/5}) \\ 0 & 0 & 0 & \frac{1}{\phi^{3/2}}(e^{4i\pi/5} - e^{-3i\pi/5}) & \frac{1}{\phi^2}e^{-3i\pi/5} + \frac{1}{\phi}e^{4i\pi/5} \end{bmatrix}, \quad (8)$$

and the next-nearest-neighbor coupling then becomes $B_i^\dagger H_{i+1} B_i$.

Similarly, for the leg coupling, illustrated for a four-leg ladder in Fig. 4, we need three braids and act on the whole sequence $|x_1,x_2,x_3,x_4,x_5,x_6\rangle$ involving six bonds (in general, involving $2W-2$ bonds for W chains) along the fusion path $\mathcal{C}$ according to the linear transformation

$$H_{\text{leg}}^{1-6} = J_{\text{leg}} B_2 \otimes B_5 \otimes B_4 \otimes \mathcal{H}_4 \otimes B_4^\dagger \otimes B_5^\dagger \otimes B_2^\dagger. \quad (9)$$

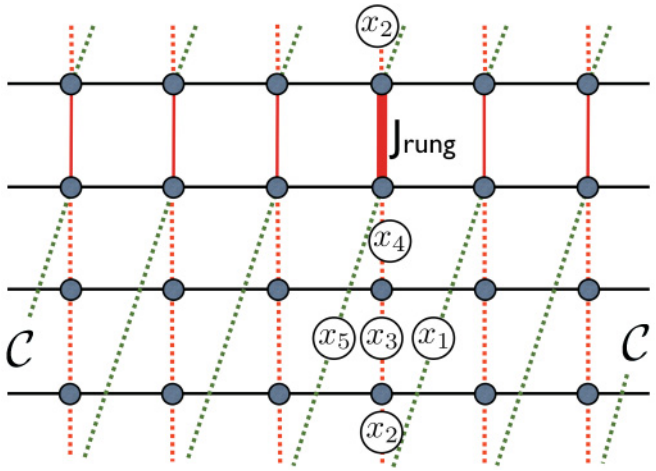

FIG. 5. (Color online) A ladder system as in Fig. 4, but with periodic boundary conditions, where an additional rung-coupling term connects the two out legs (vertical red segments).

Similar formulas can easily be derived for any bond and any width W.

It should be noticed that acting on any given initial state $|x_1 x_2 \cdots x_{LW}\rangle$, each of the $W \cdot L$ leg couplings can potentially generate up to 2^{2W-1} resulting linear independent states since each operator in (9) can generate up to two such states. This exponentially growing number of resulting states should be contrasted to the single state generated by a spin-flip operation in the case of ordinary SU(2) spins. As a consequence, this leads to denser and denser matrices for increasing W in the anyonic ladder models, which limits the numerically accessible system sizes for larger width W.

D. Periodic boundary conditions along the rungs

Closing these open boundaries along the rung direction is done by adding additional couplings between the first and last legs as shown in Fig. 5. To calculate the Hamiltonian matrix for these couplings, one first has to again braid the two involved anyons until they are nearest neighbors along the fusion path. The subtlety with this term is that after the braidings we do not end up with the usual nearest-neighbor term of Fig. 3(b), but with a coupling that twists once around the fusion path as illustrated in Fig. 3(d). Untwisting this winding by a 2π rotation of the right anyon and all following ones by 2π around the fusion path gives rise to a Dehn twist phase factor $\exp(i\Psi_x)$,[23] which is 1 for $x = \mathbf{1}$ but $\exp(-4i\pi/5)$ for $x = \tau$.

TABLE I. The various phases of the Fibonacci ladders as a function of the number of legs W. Each line corresponds to one of the four quadrants of the parameter space shown in Fig. 2. In the first column, the first (second) label refers to the rung (leg) coupling $J_{\rm rung}$ ($J_{\rm leg}$). Gapped phases are labeled by Δ. For the gapless phases the value of the central charge of the low-energy CFT is indicated.

W→	1	2	3	4	5	6
AFM-AFM	7/10	Δ	7/10	Δ	7/10	Δ
AFM-FM	4/5	Δ	4/5	Δ	4/5	Δ
FM-AFM	7/10	7/10	Δ	7/10	7/10	Δ
FM-FM	4/5	4/5	Δ	4/5	4/5	Δ

The Hamiltonian for this rung term acts on the local sites x_1,x_2,x_3,x_4,x_5 of Fig. 5 and reads

$$\tilde{H}^{1-5}_{\rm rung} = J_{\rm rung} B_2 \otimes B_3 \otimes T_4 \otimes \mathcal{H}_4 \otimes T_4^\dagger \otimes B_3^\dagger \otimes B_2^\dagger, \qquad (10)$$

where T_i is the (diagonal) 2×2 twist matrix,

$$T_i = \begin{bmatrix} 1 & 0 \\ 0 & e^{-4i\pi/5} \end{bmatrix}, \qquad (11)$$

in the local $\{|\mathbf{1}\rangle,|\tau\rangle\}$ basis (for the variable x_i).

Care must be taken in choosing a consistent convention for the phase of (counter)clockwise braids and Dehn twists. An inconsistent choice can easily be detected as it will cause a broken translation symmetry along the rungs that can be seen in, e.g., the local bond energies.

III. STRONG-COUPLING LIMIT AND PHASE DIAGRAMS

For SU(2) quantum spin ladders a single phase extends from the weak to strong rung-coupling limit for any of the four possible signs of the rung and leg couplings.[4,24] The generic phase diagram thus has at most four different phases. For the su(2)$_3$ anyonic ladder we observe the same behavior and we will start to discuss the various phases starting from the strong rung-coupling limit $|J_{\rm rung}| \gg |J_{\rm leg}|$. The results discussed below are summarized in Table I. The total spin of an isolated rung, which depends on the sign of the rung coupling and on the rung length W, completely determines the nature of the phase at finite $J_{\rm leg}$ and whether it is gapped or critical. For antiferromagnetic $J_{\rm rung}$ (first two lines of Table I) we find similar even/odd effects as in the SU(2) case. Even widths are gapped while odd widths are critical and characterized by the same conformal field theory (CFT) as the single chain. For ferromagnetic $J_{\rm rung}$ and $W = 3p$ (p an integer) the rungs form singlets (labeled with the identity $\mathbf{1}$) and hence the ladders are gapped. Otherwise, the rungs behave as "triplet" (τ) states and the low-energy physics is that of an (effective) critical chain as shown in the two last lines of Table I.

A. Antiferromagnetic rung coupling

Let us first consider AFM rung coupling, where for an isolated rung the GS has a total angular momentum $j = 0$ (state with label $\mathbf{1}$) for even width W and $j = \frac{1}{2}$ (state with label τ) for odd width.

For even W, the GS at $J_{\rm leg} = 0$ is a product of local $\mathbf{1}$ states on the individual rungs. The elementary excitation is a local triplet (τ) excitation with a gap $\Delta_0(W) \sim 1/W$. For (weak) leg coupling the elementary magnon excitation can hop to one of its two neighboring rungs in first order in $J_{\rm leg}$, giving rise to a dispersion of width $\propto|J_{\rm leg}|$. Typical such dispersions (but for intermediate couplings) are shown in Fig. 6. The gap decreases linearly as $\Delta_0(W) - \alpha|J_{\rm leg}| + O(J_{\rm leg}^2)$. However, this perturbative strong-coupling result for the gap is restricted to a shrinking region $\sim 1/W$ around $J_{\rm leg} = 0$ as W gets larger.

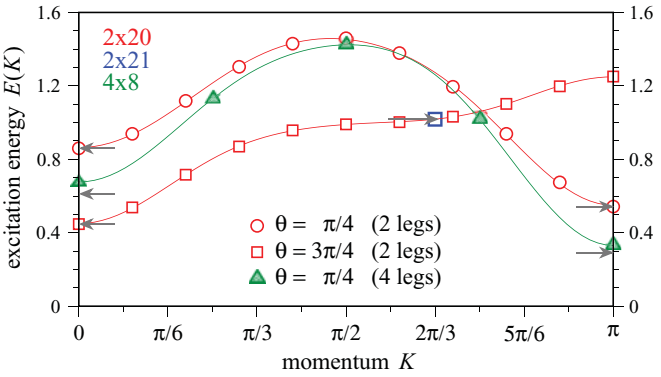

FIG. 6. (Color online) Dispersion of a generalized "magnon" excitation along the ladder direction for two-leg and four-leg ladders and various couplings. The magnon excitation is created by flipping a local label x_i from $\mathbf{1}$ to τ, which can then propagate down the ladder. Data is shown for 2×20 (and 2×21) ladders (open symbols) as well as 4×8 ladder (closed symbols) and coupling parameters $\theta = \pi/4$ ($J_{\rm leg} = J_{\rm rung} = \sqrt{1/2}$) and $\theta = 3\pi/4$ ($J_{\rm leg} = -J_{\rm rung} = -\sqrt{1/2}$). The solid lines are a guide to the eye, obtained from Fourier series fit to the data. The arrows indicate extrapolations to the thermodynamic limit as shown in Fig. 8.

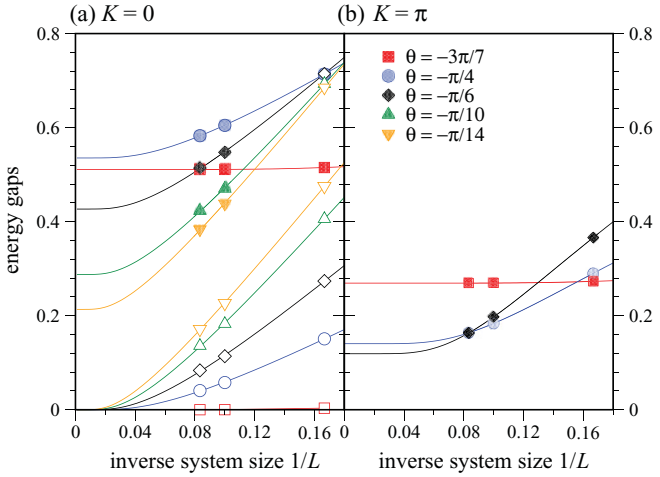

FIG. 7. (Color online) Finite-size extrapolations of the energy gaps of three-leg ladder systems for various couplings θ, with ferromagnetic rung and antiferromagnetic leg couplings in the (a) $K = 0$ and (b) $K = \pi$ momentum sectors. Extrapolations to the thermodynamic limit are obtained by fitting the numerical data to the form $\Delta(L) \simeq \Delta(\infty) + \frac{C}{L}\exp(-L/\xi)$, where ξ is a correlation length. In the $K = 0$ sector, the first excitation energy (open symbols) extrapolates to zero (indicating that the GS is twofold degenerate in the thermodynamic limit), while the extrapolation of the second excitation energy (filled symbols) indicated a finite gap.

For ordinary SU(2) ladders it has been argued that the gap vanishes as $\exp(-cW)$ for large enough W and any chain coupling $J_{\rm leg}$.[24] We will return to the question whether a gap can survive for anyonic systems in the limit $W \to \infty$ below.

Away from the above-discussed limit, the gaps of the two- and four-leg ladders can be obtained for intermediate couplings by using Lanczos exact diagonalisations of clusters of different lengths. Finite-size scalings (similar to the one shown in Fig. 7 for a three-leg ladder to be discussed later) enable to accurately estimate, in the thermodynamic limit, the gaps at the minima of the dispersion (see, e.g., Fig. 6) of the excitation spectrum. Results of the extrapolated gaps are summarized in Fig. 8(a). Note that the minima of the dispersion occurs at different momenta depending on the sign of $J_{\rm leg}$, $K = 0$, and π for antiferromagnetic $J_{\rm leg} > 0$, $K = 0$, and $2\pi/3$ for ferromagnetic $J_{\rm leg} < 0$. In the latter case, for sufficiently large leg coupling, the minima at $2\pi/3$ can disappear as shown in Fig. 6

For odd width W, since the GS of a single AFM rung carries angular momentum $j = 1/2$ (τ), the low-energy effective model for weakly coupled rungs is that of a single τ-anyon chain. Indeed, as shown in Fig. 9 for a three-leg ladder we find that the low-energy spectrum is gapless and can be described by a CFT identical to the one of a single chain.[14] In particular, we find that the lowest energies (per rung) e_n scale as

$$e_n(L) \simeq e_\infty + \pi u\left(-\frac{c}{12} + 2h_n\right)\frac{1}{L^2}, \qquad (12)$$

where L is the length of the ladder, u is a zero-mode velocity, and $2h_n$ and c are the conformal weights (or scaling

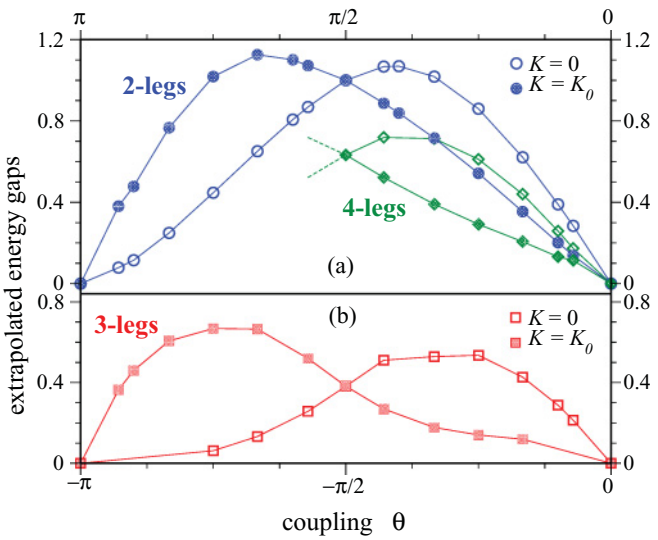

FIG. 8. (Color online) Extrapolated values $\Delta(L \to \infty)$ of the gaps at the two crystal momenta $K = 0$ and $K = K_0$ corresponding to the zero-energy modes of the single chains. $\Delta(\infty)$ is plotted as a function of coupling parameter θ, i.e., $\theta \in [0,\pi]$ for two- and four-leg ladders with AFM rung coupling (a) and $\theta \in [-\pi,0]$ for a three-leg ladder with FM rung coupling (b). For AFM (FM) leg coupling, $K_0 = \pi$ ($K_0 = 2\pi/3$) and clusters up to 2×20 (2×21), 3×12 (3×12), and 4×8 have been used. $\Delta(\infty)$ is deduced by fitting the data as $\Delta(L) \simeq \Delta(\infty) + \frac{C}{L}\exp(-L/\xi)$, where ξ is a correlation length.

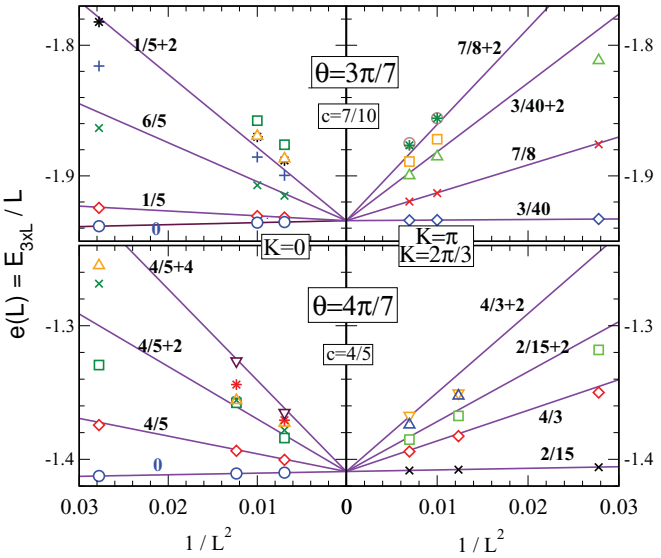

FIG. 9. (Color online) Finite-size scaling of $3 \times L$ (three-leg) ladders of sizes up to $L = 12$, with AFM rung coupling and with both AFM (top) and FM (bottom) leg couplings. The lowest eigenenergies per rung (symbols) are plotted vs $1/L^2$. The right-hand and left-hand panels correspond to two different crystal momenta, the ones characterizing the zero-energy modes of a single chain. The θ values (indicated on the plot) correspond to the strong rung couplings $|J_{\rm rung}/J_{\rm leg}| \sim 4.38$ labeled as "1" and "2" in Fig. 2. CFT scalings are shown: (i) A linear fit of the GS energy (labeled by "0") accurately provides the overall energy scale (i.e., the velocity); and (ii) all other straight lines are expected CFT scalings using the conformal weights $2h_n$ and the central charge c indicated on the plots [see Eq. (12) in the text].

dimensions) and central charge of the CFT. Depending on the sign of the leg coupling these gapless theories are those of the tricritical Ising model ($c = 7/10$) or three-state Potts model ($c = 4/5$) for AFM and FM couplings, respectively.

The anyonic ladders with AFM rung coupling thus behave similarly to their SU(2) analogs with even/odd widths giving rise to gapped and/or gapless physics as summarized in the first two lines of Table I.

B. Ferromagnetic rung coupling

Next, we move to the case of a ferromagnetic rung coupling, where we find major differences between the anyonic ladders and their SU(2) counterparts. For ordinary SU(2) ladders of even width W, the strong coupling rungs form a total integer spin and the effective low-energy model (for weak leg coupling) is a Haldane Heisenberg chain,[25] which is gapped for AFM leg coupling. For odd width W the ladders remain gapless for either sign of the leg coupling, since each rung forms a spin-1/2 state.

In contrast to the even/odd effect for ordinary SU(2) spins ladders, for anyonic ladders, we find different phases and periodicities of 3 in W for $k = 3$. Ladders with $W = 3p$ (p an integer) and ferromagnetic $J_{\rm rung}$ are gapped, since each rung forms a singlet (**1**) state similar to the even width ladders in the AFM case. As an example, we show in Fig. 8(b) the gap of a three-leg ladder obtained from finite-size scalings, examples of which are shown in Fig. 7.

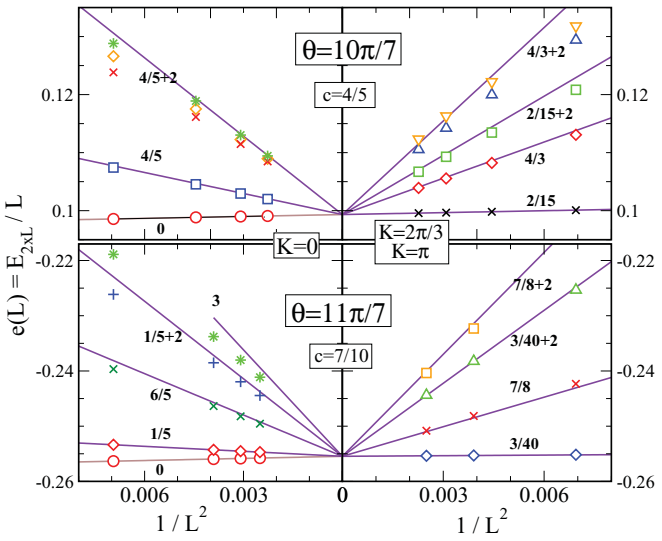

FIG. 10. (Color online) Finite-size scaling of $2 \times L$ (two-leg) ladders with FM rung coupling, with both FM (top) and AFM (bottom) leg couplings and with up to 2×21 and 2×20 sites, respectively. The θ values (indicated on the plot) correspond to the strong rung couplings $|J_{\text{rung}}/J_{\text{leg}}| \sim 4.38$ labeled as "3" and "4" in Fig. 2. Same notations and same analysis as in Fig. 9.

Alternatively, the low-energy effective model of ladders with widths that are not multiples of 3 is again that of a single τ chain and thus gapless as illustrated in Fig. 10 for a two-leg ladder. One might naively expect that the two-leg ladder is again a gapped Haldane chain, since two FM coupled $j = 1/2$ momenta form a total $j = 1$ momentum. However, as noted in the Introduction, in $\text{su}(2)_k$ theories with odd level k, one can identify momentum j with momentum $k/2 - j$ by fusing it with the Abelian momentum-$k/2$ particle. For $\text{su}(2)_3$ this implies that momentum $j = 1$ behaves as momentum $j = 1/2$ (τ). We find that this gapless phase extends all the way up to weak rung coupling.

We summarize our results in the phase diagrams of Fig. 11(a) for two-leg and four-leg ladders, and of Fig. 11(b) for three-leg ladders.

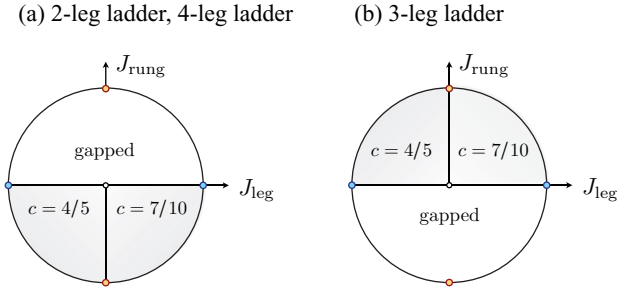

FIG. 11. (Color online) Phase diagrams of the two-leg and four-leg ladders (a) and of the three-leg ladders (b) vs the couplings $J_{\text{leg}} = \cos\theta$ and $J_{\text{rung}} = \sin\theta$. The central charge of the gapless phases is indicated.

IV. DECOUPLED CHAINS

We now turn to a discussion of the limit where the rung coupling between the individual legs of the ladder vanishes. In contrast to the case of conventional SU(2) spin ladders, we find that the anyonic ladder system does *not* decompose into independent chains in this limit of vanishing rung coupling, i.e., $J_{\text{rung}} = 0$. In particular, we find that the energy spectrum in this limit is *not* given by the free tensor product of the energy spectra of individual chains, but rather turns out to be a certain subset thereof. In the following, we describe a set of "topological gluing conditions" that constrain the energy spectrum to this subset of the free tensor product. We closely follow the analytical arguments, which we developed in Refs. 16 and 21 in a so-called "liquids picture," where we identify the collective gapless modes of the quasi-1D anyon chains (or ladders) with edge states at the spatial interface between two distinct topological quantum liquids—for an illustration see, e.g., Fig. 2 of Ref. 16. This liquids picture provides a set of analytical rules which allow to obtain the spectrum of these decoupled anyon chains, which in the remainder of this section we compare with numerical results for two-leg and three-leg ladder systems. We find perfect agreement of the two approaches.

Let us briefly describe the analytical spectrum of the decoupled chains ($J_{\text{rung}} = 0$ limit), based on the results obtained in Ref. 16 (see Fig. 2 of that reference). At each interface between two topological (or Hall) liquids there is an edge [see Fig. 2(b) of Ref. 16]. The key tool developed in Ref. 16 was that each chain can be viewed as "filled" with a new topological (or Hall) liquid so that the right- and left- moving gapless degrees of freedom of each chain arise from the juxtaposition of two topological liquids. The field theory describing each of these edges arises from the familiar Goddard-Kent-Olive (GKO) coset construction[26] of CFT. Consider for example two decoupled chains. Thus, there are five liquids, and four edges. For, say, AF interactions between the anyons, the spectrum of these four edges in the "topological sector" of "topological charge" j_1 takes on the form (following the rules developed in Ref. 16, and using the notation of the same article)

$$(\psi_L)^{j_1}_{j_2}\,(\psi_R)^{j_1'}_{j_2}\,(\psi_L)^{j_1'}_{j_2'}\,(\psi_R)^{j_1}_{j_2'}.$$

Here j_1 denotes the topological charge which is "ejected" from the four-edge system to infinity through the surrounding ("parent") topological liquid [compare again Fig. 2(b) of Ref. 16]. The left (holomorphic) and right (antiholomorphic) conformal weights of this state are

$$h_L = \Delta^{j_1}_{j_2} + 0 + \Delta^{j_1'}_{j_2'} + 0, \tag{13}$$

$$h_R = 0 + \Delta^{j_1'}_{j_2} + 0 + \Delta^{j_1}_{j_2'}, \tag{14}$$

respectively, where $\Delta^{j_1}_{j_2} = [1 + j_2(j_2+1)/(k+1) - j_1(j_1+1)/(k+2)]$ is the conformal weight of the primary field $(\psi_L)^{j_1}_{j_2}$ in the GKO coset $\text{su}(2)_{k-1} \times \text{su}(2)_1/\text{su}(2)_k$. Considering for simplicity $k =$ odd, we can choose j_1 and j_1' to run over integer values $0, 1, \ldots, (k-1)/2$ and j_2, j_2' run over values $0, 1/2, 1, \ldots, (k-1)/2$. We are only interested in fields with

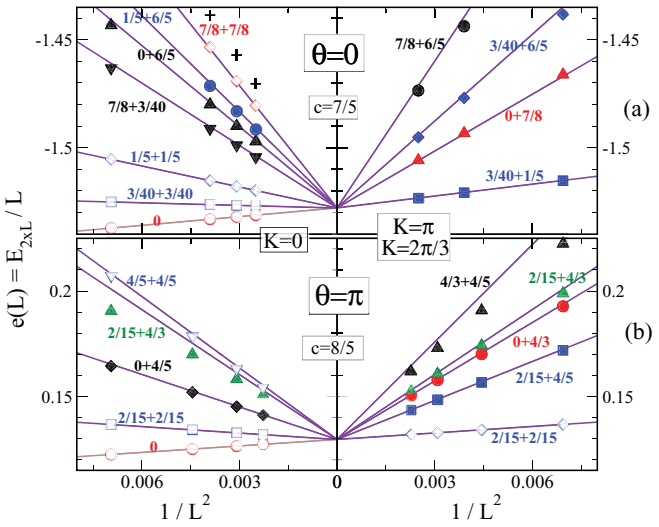

FIG. 12. (Color online) Finite-size scaling of the lowest eigenenergies (normalized per rung) of a two-leg ladder with $J_{\text{rung}} = 0$ and $J_{\text{leg}} = \pm 1$ (decoupled chains) vs $1/L^2$. The right-hand and left-hand panels correspond to two different crystal momenta, the ones characterizing the zero-energy modes of a single chain. Same procedure and notations as Figs. 9 and 10.

$h_L = h_R$, so that the scaling dimension is $x(j_1; j_2; j_1'; j_2'; j_1) = 2h_L$.

We now compare the above analytical spectrum with numerical spectra for decoupled chains. Finite-size scaling of the low-energy spectrum (similar to the procedure employed in the previous section) enables us to assign conformal weights to each energy level, analogous to the case of the two-leg $su(2)_3$ ladder in Fig. 12. As before, an accurate fit of the GS energy per site versus $1/L^2$ fixes the overall energy scale. The (allowed) combinations $2h_L = 2h_1 + 2h_2$ corresponding to the sum of two conformal weights, each arising from a single edge state [compare Eq. (13)], can then be read off from the slopes of the lowest excited states versus $1/L^2$. These numerical results as well as those for three decoupled legs (scaling not shown here), and for both FM and AFM (intraleg) couplings, are summarized in Table II. The quantum numbers (and degeneracies) obtained numerically are in perfect agreement with those obtained from the above analytical analysis.

V. EFFECTS OF BOUNDARY CONDITIONS

A characteristic feature of a topological phase is that it is sensitive to the topology of the underlying manifold,[27] which is reflected in a nontrivial GS degeneracy and the occurrence of gapless edge modes for open boundaries. In this section, we will investigate the sensitivity of the anyon ladder systems to these latter effects of changing boundary conditions. So far we considered anyon ladder systems with open boundary conditions along the rung direction and periodic boundary conditions along the leg directions, resulting in the topology of an annulus. Following the arguments in Refs. 16 and 21 we interpret the observation of gapless states in the energy spectrum as the appearance of gapless *edge modes* at the open boundary conditions. As a consequence, we expect the energy spectrum to gap out as we remove the gapless edge states by gluing together the open boundaries of the annulus to yield a torus geometry. As detailed in Sec. II D this topology change is accomplished by adding a rung coupling between the two outer legs of the ladder (and introducing the correct Dehn twist).

TABLE II. Scaling dimensions for two (top) and three (bottom) decoupled chains with AFM ($\theta = 0$) and FM ($\theta = \pi$) leg couplings, for the two crystal momenta corresponding to the respective zero-energy modes of a single chain. Listed here are the numerically observed conformal operators in the subset of the free-tensor product of energy states for W individual chains, corresponding to CFTs with central charge $c = W \times \frac{7}{10}$ ($c = W \times \frac{4}{5}$) for AFM (FM) coupling. For the Ising theory ($c = 7/10$), we use the common identification of operators with conformal weights, i.e., $I \to 0$, $\epsilon \to 1/5$, $\epsilon' \to 6/5$, $\epsilon'' \to 3$, $\sigma \to 3/40$, $\sigma' \to 7/8$. For the three-state Potts model ($c = 4/5$) this identification becomes $I \to 0$, $\epsilon \to 4/5$, $\sigma_{1,2} \to 2/15$, $\psi_{1,2} \to 4/3$. For the case of two chains we also list the topological symmetry sector, i.e., the eigenvalue of the topological symmetry operator, for all energies.

Two-leg ladder

$\theta = 0$ $K = 0$	Top. sector	$\theta = 0$ $K = \pi$	Top. sector	$\theta = \pi$ $K = 0$	Top. sector	$\theta = \pi$ $K = 2\pi/3$	Top. sector
I	0	$\sigma + \epsilon$	$(\frac{1}{2}, \frac{1}{2})$	I	0	$\sigma + \sigma$	$\frac{1}{2}$
$\sigma + \sigma$	$\frac{1}{2}$	$I + \sigma'$	0	$\sigma + \sigma$	$\frac{1}{2}$	$\sigma + \epsilon$	$(\frac{1}{2}, \frac{1}{2})$
$\epsilon + \epsilon$	$\frac{1}{2}$	$\sigma + \epsilon'$	$(\frac{1}{2}, \frac{1}{2})$	$I + \epsilon$	$(0, \frac{1}{2})$	$I + \psi$	(0,0)
$\sigma + \sigma'$	$(0, \frac{1}{2})$	$\sigma' + \epsilon'$	$(0, \frac{1}{2})$	$\sigma + \psi$	$(0,0, \frac{1}{2}, \frac{1}{2})$	$\sigma + \psi$	$(0,0, \frac{1}{2}, \frac{1}{2})$
$I + \epsilon'$	$(0, \frac{1}{2})$			$\epsilon + \epsilon$	$\frac{1}{2}$	$\epsilon + \psi$	$(0, \frac{1}{2})$
$\epsilon + \epsilon'$	$(\frac{1}{2}, \frac{1}{2})$						
$\sigma' + \sigma'$	0						

Three-leg ladder

$\theta = 0$ $K = 0$	$\theta = 0$ $K = \pi$	$\theta = \pi$ $K = 0$	$\theta = \pi$ $K = 2\pi/3$
I	$\sigma + \sigma + \sigma$	0	$\sigma + \sigma + \sigma$
$\sigma + \sigma + \epsilon$	$\epsilon + \epsilon + \sigma$	$I + \sigma + \sigma$	$I + \sigma + \epsilon$
$\epsilon + \epsilon + \epsilon$	$I + I + \sigma'$	$I + I + \epsilon$	$I + I + \psi$
$I + \sigma + \sigma'$		$\sigma + \sigma + \epsilon$	

As an example system we consider a four-leg ladder with FM rung coupling $J_{\text{rung}} < 0$. In the case of open boundary conditions along the rung direction, we find clear signatures for gapless edge modes at these open boundaries: First, the energy spectrum is gapless in the thermodynamic limit as shown in Fig. 13. The energy eigenvalues again agree well with the expected conformal weights, both in the strong and intermediate coupling regimes shown in Figs. 13(c) and 13(a), respectively. Second, correlations of the bond-energy operator decrease significantly *slower* between two bonds located on the two *outer* legs than on the *inner* legs as shown in Fig. 14. In addition, the bond-bond energy correlations on the *rungs* in both the two outer rows and the inner row of the four-leg ladder decay more rapidly that their leg counterparts. We interpret these differences as evidence for a gapless edge mode being located at the open boundaries of the ladder system and the presence of a gap in the bulk.

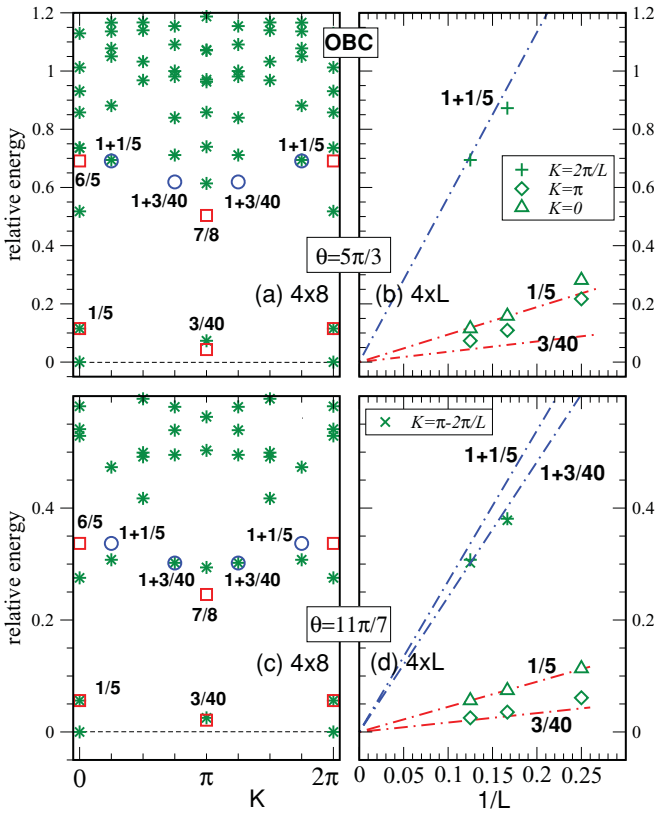

FIG. 13. (Color online) Low-energy excitations of four-leg ladders with open boundary conditions. The GS energy (K=0) is used as energy reference. FM (AFM) rung (leg) coupling are considered, i.e., giving rise to the $c = 7/10$ phase of Fig. 11(a): Moderately strong rung coupling, $|J_{\text{rung}}|/J_{\text{leg}}| \sim 1.73$ ($\theta = 5\pi/3$), and strong rung coupling, $|J_{\text{rung}}|/J_{\text{leg}} \sim 4.38$ ($\theta = 11\pi/7$), are shown. (a), (c) Low-energy spectra of a 4×8 ladder vs momentum along the ladder. (b), (d) Finite-size scalings of the low-energy levels for the two cases shown in (a) and (c). Fits to $c = 7/10$ CFT invariant spectra are provided: Expected levels corresponding to primary (secondary) fields of the CFT are shown by red boxes (blue circles). The overall energy scale of the CFT is set by adjusting the position of the $K = 0, 2h = 1/5$ state to the corresponding energy level of the 4×8 cluster.

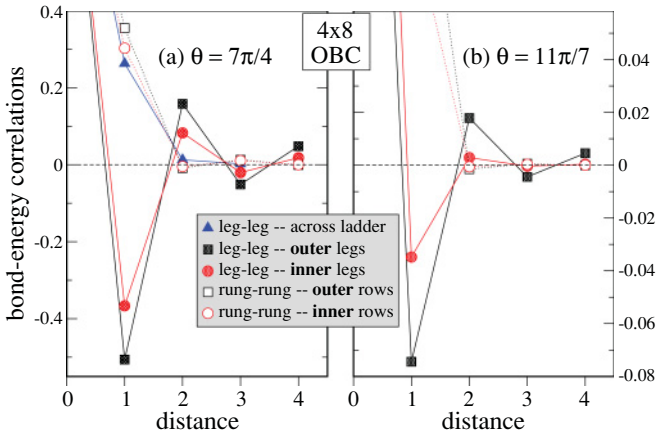

FIG. 14. (Color online) Bond-energy correlations in a 4×8 ladder with open boundary conditions (OBC) along the rungs (i.e., with two inner and two outer eight-site legs) as a function of the distance between two (parallel) bonds along the leg direction or across the ladder. The bonds are oriented simultaneously along the rungs (rung-rung correlator) or along the legs (leg-leg correlator). The disconnected part has been subtracted and the data are normalized with regard to the zero-distance autocorrelation. Data are shown for $J_{\text{rung}} < 0$ and $J_{\text{leg}} > 0$, i.e., in the $c = 7/10$ phase of Fig. 11(a). (a) Isotropic couplings, $|J_{\text{rung}}|/J_{\text{leg}} = 1$ ($\theta = 7\pi/4$); (b) strong rung coupling, $|J_{\text{rung}}|/J_{\text{leg}} \sim 4.38$ ($\theta = 11\pi/7$).

The occurrence of the bulk gap of this anyon ladder system becomes even more evident when we consider the energy spectrum as we close the open boundary conditions, thereby removing the gapless (edge) modes. In Fig. 15 we show such clearly gapped energy spectra for periodic boundary conditions (in the intermediate coupling regime $\theta = 5\pi/3$ and $\theta = 7\pi/4$). This observation should be contrasted with our results for open boundary conditions and the same coupling parameters: As shown in Figs. 13(a) and 13(b), for the same coupling parameter $\theta = 5\pi/3$ the energy spectrum in the case of open boundary conditions nicely matches the gapless spectrum of a CFT.

Furthermore, the gapped energy spectrum for periodic boundary conditions, as illustrated in Fig. 15, also reveals the occurrence of an unusual, nontrivial GS degeneracy for the anyonic ladder system. For example, in the case of FM rung coupling $J_{\text{rung}} < 0$ and AFM leg coupling $J_{\text{leg}} > 0$, we observe three GSs (by changing the initial conditions of the Lanczos exact diagonalization procedure, we have checked that each of these levels corresponds indeed to a *single* energy eigenstate) (one at momentum 0 and two at momentum π) separated from the rest of the energy spectrum by a gap of order $O(1)$ in the exchange coupling strength, which become degenerate in the thermodynamic limit. Evidence for the latter is provided in the finite-size scaling plots of Figs. 15(b) and 15(d). It is important to notice that such a GS degeneracy is *not* due to a spontaneous dimerization along the ladder direction (or to any other spontaneous translation symmetry breaking). Indeed, in the case of a spontaneous dimerization, the expected GS degeneracy would be a multiple of two (depending on whether the system breaks translational invariance along both ladder directions) instead of three for the anyon ladder.

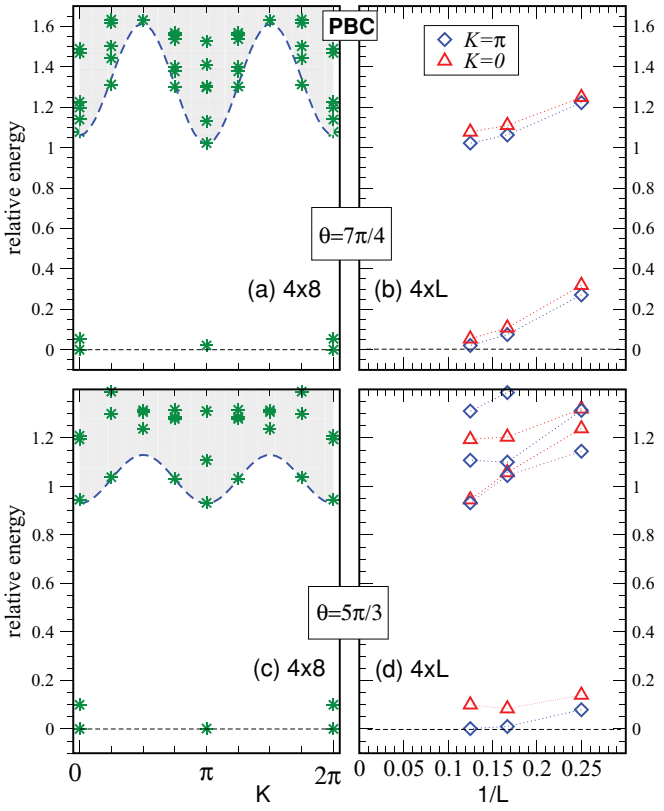

FIG. 15. (Color online) Low-energy excitations of four-leg ladders with periodic boundary conditions. The GS energy (K=0) is used as energy reference. (a), (c) Spectra of a 4×8 ladder for values of θ corresponding to FM (AFM) rung (leg) coupling. Isotropic couplings, $|J_{\rm rung}|/J_{\rm leg} = 1$ ($\theta = 7\pi/4$), and moderately strong rung coupling, $|J_{\rm rung}|/J_{\rm leg} \sim 1.73$ ($\theta = 5\pi/3$), are shown. (b), (d) Finite-size scalings of the low-energy levels for the two cases shown in (a) and (c) revealing threefold degenerate GSs and a finite gap.

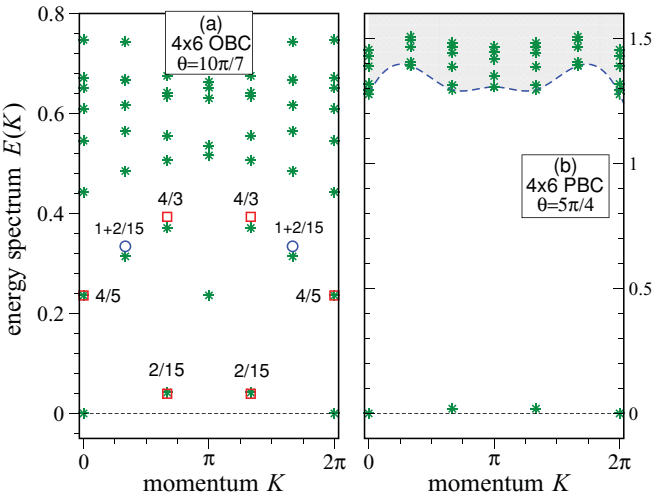

FIG. 16. (Color online) Low-energy excitations of 4×6 ladders with FM rung and leg couplings. The GS energy ($K = 0$) is used as energy reference. (a) Open boundary condition (in the rung direction). The data are obtained for strong rung coupling, $J_{\rm rung}/J_{\rm leg} \sim 4.38$ ($\theta = 10\pi/7$). A fit to a $c = 4/5$ CFT invariant spectrum is shown: Expected levels corresponding to primary (secondary) fields of the CFT are represented by red boxes (blue circles) and the overall energy scale is set by adjusting the position of the $K = 0$, $2h = 4/5$ energy level. (b) Periodic boundary condition (in the rung direction). The data are obtained for isotropic couplings, $J_{\rm rung}/J_{\rm leg} = 1$ ($\theta = 5\pi/4$). A large gap is seen above three quasidegenerate levels.

Further evidence for a uniform anyon GS is provided by inspection of the correlations of the energy (rung or leg) bond operators shown in Fig. 17 for the same periodic anyon ladder. While for a dimerized system (period-2) oscillations of these correlations survive at arbitrarily large separations between the bonds (the amplitude is the square of the order parameter for infinite separation), our data show in contrast a rapid vanishing of those oscillations with distance.

Similarly, we have also checked that the spectrum of a 4×6 ladder with both ferromagnetic rung and leg couplings, $J_{\rm rung} < 0$ and $J_{\rm leg} < 0$, is fully consistent with (i) a $c = 4/5$ CFT invariant spectrum when open boundaries are used, most evidently seen for strong rung coupling in Fig. 16(a) and (ii) a gapped spectrum and a threefold degenerate GS with momenta 0 and $\pm 2\pi/3$ is found when using *periodic* boundary conditions (i.e., removing the edges), most evidently seen for isotropic couplings in Fig. 16(b). Again, this degeneracy is *not* connected to translation symmetry breaking but rather is a signature of a new (uniform) topological liquid. This behavior of the anyon ladder systems should be contrasted to the case of conventional SU(2) spin ladders. First, SU(2) spin ladders with an even number of legs always exhibit a gap (apart for the case of simultaneous FM rung and leg couplings for which the GS is a trivial fully polarized ferromagnet). Second, ladders with an odd number of legs are always gapless if open boundary conditions are used along the rung direction. When periodic boundary conditions along the rung direction are used to form so-called spin tubes[28] with an odd number of legs, dimerization in the leg direction generically sets in if the rung exchange coupling is AFM.

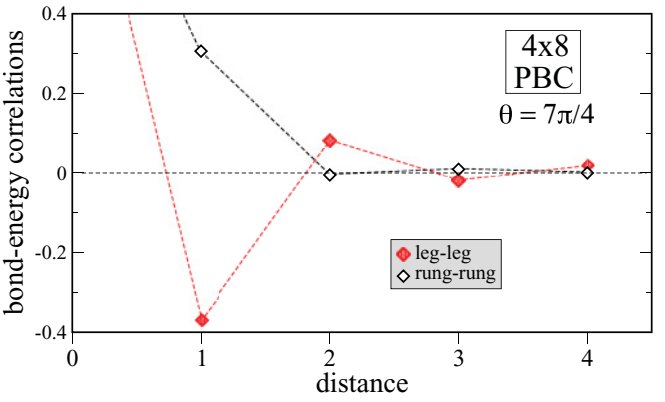

FIG. 17. (Color online) Bond-energy correlations in a 4×8 ladder with *periodic* boundary conditions (PBC) along the rungs as a function of the distance (in the leg direction) between two (parallel) bonds. The bonds are oriented simultaneously along the rungs (rung-rung correlator) or along the legs (leg-leg correlator). The disconnected part has been subtracted and the data are normalized with regard to the zero-distance autocorrelation. Data are shown for $J_{\rm rung} < 0$ and $J_{\rm leg} > 0$, i.e., in the $c = 7/10$ phase of Fig. 11(a) and for isotropic couplings, $|J_{\rm rung}|/J_{\rm leg} = 1$ ($\theta = 7\pi/4$).

TABLE III. GS angular momentum (i.e., total spin) of a single *FM* $su(2)_k$ rung as a function of its length W (first line) and k (first column). The last line gives the GS total spin of FM Heisenberg SU(2) open chains of same lengths. When small J_{leg} is switched on, the corresponding W-leg ladders can be mapped onto single gapless effective chains (at low energies) except for the cases (i) marked by boxes (Haldane effective chains) or (ii) marked by "**0**" (i.e., when the GS of a single rung is a singlet). The vertical bars ‖ indicate the range $W < k/2$ (see text).

$k \setminus W$	1	2	3	4	5	6	7	8	9
3	1/2 ‖	1/2	**0**	1/2	1/2	**0**	1/2	1/2	**0**
5	1/2	$\boxed{1}$ ‖	$\boxed{1}$	1/2	**0**	1/2	$\boxed{1}$	$\boxed{1}$	1/2
7	1/2	$\boxed{1}$	3/2 ‖	3/2	$\boxed{1}$	1/2	**0**	1/2	$\boxed{1}$
9	1/2	$\boxed{1}$	3/2	$\boxed{1}$ ‖	$\boxed{2}$	3/2	$\boxed{1}$	1/2	**0**
⋮	...								
∞	1/2	$\boxed{1}$	3/2	$\boxed{2}$	5/2	$\boxed{3}$	7/2	$\boxed{4}$	9/2

VI. $su(2)_k$ GENERALIZATIONS

We now turn to the question of how the characteristic features of the W-leg ladder models found for the Fibonacci theory $su(2)_3$ are generalized when considering $su(2)_k$ theories with $k > 3$. All these theories allow to define ladder models built out of generalized angular momenta $j = 1/2$, similar to the description given in Sec. II. For these more general theories we can identify angular momentum j with angular momentum $k/2 - j$ with the highest possible allowed angular momentum thus becoming $(k-1)/4$ when k is odd.

Following the same route as taken for the Fibonacci theory, we can access most features of their respective phase diagrams by considering the strong rung-coupling limit as presented in Sec. III. In particular, such an approach reveals the appearance of gapped and gapless phases as a function of the ladder width W and the level k. For AFM rung coupling $J_{\text{rung}} > 0$ we find that the odd/even effect of $su(2)_3$ occurs for all level k. On the other hand, for FM rung coupling $J_{\text{rung}} < 0$ a more refined picture emerges: If the ladder width W is a multiple of the level k, i.e., $W = 0 \bmod k$, the total angular momentum on a rung is $j = 0$ and we find gapped phases around this strong rung-coupling limit. If the ladder width W is not a multiple of the level k, i.e., $W \neq 0 \bmod k$, then we still expect gapped phases if the total angular momentum on a rung is an integer (thus giving rise to generalized Haldane phases[16]). Similarly, we expect that gapless phases are found for a total angular momentum on a rung becoming a half-integer (and W not a multiple of k). These results are summarized in Table III.

This scenario also matches nicely the well-known behavior of ordinary SU(2) ladder models, which we recover when taking the limit of $k \to \infty$ for the anyonic theories.

VII. APPROACHING THE 2D LIMIT

We conclude with a perspective on how to connect the results obtained here for W-leg ladders to the thermodynamic limit of 2D lattice configurations of non-Abelian anyons. The strong rung-coupling limit, which was useful to discuss the phases of W-leg ladders, turns out to be of little help in understanding this 2D limit. The reason is that the gap of an isolated rungs vanishes as $1/W$ with increasing width, which restricts the applicability of the perturbative argument around the strong rung-couling limit to a regime of couplings $J_{\text{leg}}/J_{\text{rung}} < O(1/W)$, which also vanishes as $W \to \infty$.

Instead we consider the following general symmetry argument: In contrast to their ordinary SU(2) counterpart, the $su(2)_k$ anyonic theories lack a built-in continuous symmetry. In the assumed absence of an emergent continuous symmetry this reduces their ability to undergo a spontaneous symmetry breaking transition—such as, in 2D, the formation of a Néel state and its gapless Goldstone mode for ordinary SU(2) quantum magnets. Therefore, one is naturally led to expect gapped quantum GSs, such as topological quantum liquids, in these anyonic systems. This raises the question of how these two seemingly disjunct scenarios for SU(2) and $su(2)_k$ can be reconciled when taking the $k \to \infty$ limit of the anyonic theories. Noting that the deformation of SU(2) used to describe the anyonic systems explicitly breaks time-reversal symmetry, we can think of $1/k$ as the strength of a symmetry breaking field. As such we expect the bulk gap of the 2D anyonic quantum GS to close as one approaches the SU(2) limit, thereby smoothly connecting the topological quantum liquids to the Néel state.

The formation of a gapped bulk liquid in the thermodynamic limit is further backed by the liquids picture presented in Ref. 21. There we have argued that the interactions between a set of non-Abelian anyons arranged on a 2D lattice gives rise to the nucleation of a unique bulk-gapped (i.e., topological) quantum liquid within the parent liquid of which the anyons are excitations of. At the spatial interface between these two distinct, bulk-gapped phases gapless edge modes will form whose precise character can be identified from the gapless modes of 1D chains of anyons,[16] which in turn allows for an identification of the newly formed 2D bulk-gapped liquid.[21] For the case that both the rung and leg couplings are AFM, i.e., $J_{\text{rung}} > 0$ and $J_{\text{leg}} > 0$, this liquid is described by a $su(2)_{k-1} \times su(2)_1$ Chern-Simons theory. On the other hand, if both couplings are FM, i.e., $J_{\text{rung}} < 0$ and $J_{\text{leg}} < 0$, then this liquid is described a $U(1)$ Chern-Simons theory. The case of mixed coupling signs remains open.

Anyonic generalizations of quantum magnets in the spirit of the work presented here can be discussed in analogous fashion for other anyonic theories (tensor categories) and for other 2D lattice geometries and interactions. We expect this to be a

fruitful and broad field of research at the interface of quantum magnetism and topological states of matter.

ACKNOWLEDGMENTS

We thank Z. Wang for insightful discussions. D.P. was supported by the French National Research Agency (ANR), A.W.W.L., in part, by NSF DMR-0706140, and M.T. by the Swiss National Science Foundation. We acknowledge hospitality of the Aspen Center for Physics, the Max-Planck Institute for the Physics of Complex Systems, Dresden, and the Kavli Institute for Theoretical Physics supported by NSF PHY-0551164.

[1] T. Giamarchi, *Quantum Physics in One Dimension* (Oxford University Press, Oxford, 2004).
[2] J. D. Reger and A. P. Young, Phys. Rev. B **37**, 5978 (1988).
[3] S. R. White and D. J. Scalapino, Phys. Rev. Lett. **91**, 136403 (2003), and references therein.
[4] For a review, see E. Dagotto and T. M. Rice, Science **271**, 618 (1996), and references therein.
[5] M. Azuma, Z. Hiroi, M. Takano, K. Ishida, and Y. Kitaoka, Phys. Rev. Lett. **73**, 3463 (1994).
[6] N. Read and D. Green, Phys. Rev. B **61**, 10267 (2000).
[7] G. Moore and N. Read, Nucl. Phys. B **360**, 362 (1991).
[8] P. Bonderson and J. K. Slingerland, Phys. Rev. B **78**, 125323 (2008).
[9] R. Ilan, E. Grosfeld, K. Schoutens, and A. Stern, Phys. Rev. B **79**, 245305 (2009), and references therein.
[10] L. Fu and C. L. Kane, Phys. Rev. Lett. **100**, 096407 (2008).
[11] See, e.g., N. R. Cooper, N. K. Wilkin, and J. M. F. Gunn, Phys. Rev. Lett. **87**, 120405 (2001).
[12] C. Nayak, S. H. Simon, A. Stern, M. Freedman, and S. Das Sarma, Rev. Mod. Phys. **80**, 1083 (2008).
[13] See, for instance, C. Kassel, *Quantum Groups* (Springer, New York, 1995).
[14] A. Feiguin, S. Trebst, A. W. W. Ludwig, M. Troyer, A. Kitaev, Z. Wang, and M. H. Freedman, Phys. Rev. Lett. **98**, 160409 (2007).
[15] S. Trebst, E. Ardonne, A. Feiguin, D. A. Huse, A. W. W. Ludwig, and M. Troyer, Phys. Rev. Lett. **101**, 050401 (2008).
[16] C. Gils, E. Ardonne, S. Trebst, A. W. W. Ludwig, M. Troyer, and Z. Wang, Phys. Rev. Lett. **103**, 070401 (2009).
[17] E. Ardonne, J. Gukelberger, A. W. W. Ludwig, S. Trebst, and M. Troyer, New J. Phys. **13**, 045006 (2011).
[18] N. E. Bonesteel and K. Yang, Phys. Rev. Lett. **99**, 140405 (2007).
[19] L. Fidkowski, G. Refael, N. E. Bonesteel, and J. E. Moore, Phys. Rev. B **78**, 224204 (2008).
[20] L. Fidkowski, H.-H. Lin, P. Titum, and G. Refael, Phys. Rev. B **79**, 155120 (2009).
[21] A. W. W. Ludwig, D. Poilblanc, S. Trebst, and M. Troyer, New J. Phys. **13**, 045014 (2011).
[22] S. Trebst, M. Troyer, Z. Wang, and A. W. W. Ludwig, Prog. Theor. Phys. Suppl. **176**, 384 (2008).
[23] Andrew J. Casson and Steven A Bleiler, *Automorphisms of Surfaces After Nielsen and Thurston* (Cambridge University Press, Cambridge, UK, 1988).
[24] M. Greven, R. J. Birgeneau, and U.-J. Wiese, Phys. Rev. Lett. **77**, 1865 (1996), and references therein.
[25] F. D. M. Haldane, Phys. Rev. Lett. **50**, 1153 (1983).
[26] P. Goddard, A. Kent, and D. Olive, Commun. Math. Phys. **103**, 105 (1986).
[27] X.-G. Wen, Phys. Rev. B **40**, 7387 (1989).
[28] H. J. Schulz, in *Correlated Fermions and Transport in Mesoscopic Systems*, edited by T. Martin, G. Montambaux, and J. Tran Than Van (Editions Frontiers, Gif-sur-Yvette, 1996), p. 81; K. Kawano and M. Takahashi, J. Phys. Soc. Jpn. **66**, 4001 (1997).